Bit-Flipping Helper-Assisted Lossy Communications: Performance Analyses over Fading Multiple Access Channels

Wensheng Lin, *Member, IEEE*, Amin Zribi, *Senior Member, IEEE*, Reza Asvadi, *Senior Member, IEEE*, Elsa Dupraz, *Member, IEEE*, Lixin Li, *Member, IEEE*, and Tad Matsumoto, *Life Fellow, IEEE*

***Abstract*— The primary objective of this paper is to establish an analytical framework for evaluating the rate-distortion and the outage probability performance in Internet-of-Things (IoT) systems based on lossy cooperative wireless communications. Two correlated sources transmit information through fading multiple access channels (MACs) with the assistance of a bit-flipping (BF) helper. To begin with, we derive a closed-form expression of the inner bound on the achievable rate-distortion region. To reduce computational complexity, we then propose an approximate method for calculating the outage probability based on the lossy source-channel separation theorem. Moreover, Monte-Carlo methods are adopted to evaluate the outage probability in MAC and orthogonal transmission schemes. Theoretically approximate results are also compared with the exact results obtained by Monte-Carlo methods. It is shown that the gap between the approximate and exact performance curves decreases as the distortion requirement becomes smaller. Especially when the distortion requirement reduces to zero, the approximated outage probability is exactly the same as the results obtained by Monte-Carlo methods. In addition, we also present performance comparisons in terms of the outage probability between Rayleigh and Nakagami-m fading, and between BF helper and optimal helper.**

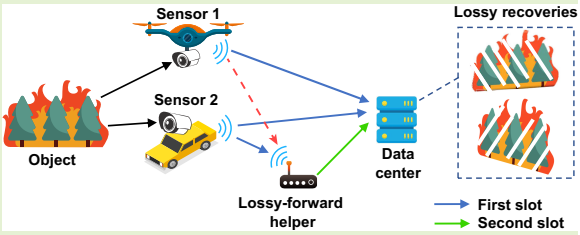

***Index Terms*— Wireless sensor networks, cooperative lossy communications, outage probability, rate-distortion, multiple access channel.**

I. Introduction

In wireless sensor networks (WSNs) and Internet-of-Things (IoT) systems, sensors located at different places, in many cases, monitor the same object or the same area [1]. Therefore, the information collected by several sensors is correlated. Undoubtedly, performance of the IoT systems can be enhanced by exploiting the correlation knowledge among the collected information [2].

In wireless IoT systems, the received information is, in many cases, not lossless due to the detrimental effect of fading variations in the wireless channels. In conventional approaches, the error-corrupted information is usually discarded. However, most often, the final objective of IoT is not only to recover the information but rather to apply a particular task on the received data, such as decision making [3]. Such paradigm may allow one to exploit lossy information as long as the system can make the correct decisions. Backed by the current strong tendency for effective utilizing deep neural network (DNN), the new paradigm has been further inherited to the new technological trend such as cloud radio access networks (CRAN) [4] and multi-view learning [5]. In this paper, we refer to this as the lossy-communication-accurate-decision principle.

Besides, the lossy-communication-accurate-decision network design concept has attracted great attention in the emerging field of goal-oriented communications, where the receiver's roles include computing, learning, quantization, etc., instead of data reconstruction alone. For example, by exploiting lossy communications for feature sharing, vehicular cooperative perception can achieve obviously higher detection performance [6]. In addition, the decision making and learning performance has been shown to directly depend on the distortion [7], [8]. Moreover, Stavrou and Kountouris [9] investigate goal-oriented communications through rate-distortion theory, by considering several different distortion criteria. Nonetheless, the results in [9] are only for point-to-point communications, and hence this paper aims at the more

W. Lin and L. Li are with the School of Electronics and Information, Northwestern Polytechnical University, Xi'an, Shaanxi 710129, China (e-mail: linwest@nwpu.edu.cn; lilixin@nwpu.edu.cn).

A. Zribi is with the ICT Department of ISETCom, Ariana, Tunisia, and also with IMT Atlantique Bretagne Pays de la Loire, 29238 Brest, France (e-mail: amin.zribi@isetcom.tn).

R. Asvadi is with the Department of Telecommunications, Faculty of Electrical Engineering, Shahid Beheshti University, Tehran 1983963113, Iran (e-mail: r_asvadi@sbu.ac.ir).

E. Dupraz is with the Lab-STICC, IMT Atlantique, Université Bretagne Loire (UBL), 29238 Brest, France (e-mail: elsa.dupraz@imt-atlantique.fr).

T. Matsumoto is with IMT Atlantique Bretagne Pays de la Loire, 4 Rue Alfred Kastler, 44300 Nantes, France, and also with the Centre for Wireless Communications, University of Oulu, 90014 Oulu, Finland (e-mail: tadashi.matsumoto@imt-atlantique.fr).

general case of cooperative communications.

To identify the design criteria towards establishing the lossy-communication-accurate-decision network design techniques, this paper considers a small, still yet generic cooperative IoT network scenario, as shown in the graphical abstract, where two sensors monitor the same object from different positions. This framework does not limit sensor types or power consumptions. The results of this paper can be applied in many different scenarios, including video surveillance, smart agriculture, climate data collection, etc.; how the results can be applied is the matter of system modeling. Therefore, the sensor type and power consumptions depend on the application scenario, and hence are not specified in our analysis. The correlated observations of the common single *event* are then sent to a data center, which aims to make accurate decisions based on the lossy reconstructions. The loss is defined by the average distortions following a proper distortion measure. We consider that if the lossy recoveries satisfy the specified distortion requirements, the system can make accurate decisions. Thus, the outage event is defined as that the distortion requirements are not satisfied for at least one link.

For the lossy-communication-accurate-decision network, to improve the decision accuracy and to reduce outage probability, a helper-assisted transmission scheme is introduced in [13] where the helper best exploits the observed information in an optimal way as suggested by the data processing theorem [27, Theorem 2.8.1]. It is shown in [13] that introducing the optimal helper can significantly improve the communication reliability and reduce the outage probability. However, the work in [13] does not show a practical structure of the optimal helper.

The primary objective of this paper is to establish for a practical structure of helper-assisted IoT networks an analytical framework for evaluating the rate-distortion and the outage probability performance. A helper is utilized between Sensor 2 (see the graphical abstract) and the data center to forward an observation copy[1], which could be corrupted by errors. To reduce the required transmission time slots, multiple access channels (MACs) are assumed for the Sensor-to-Helper as well as Sensor-to-Center transmissions, both at the first time slot. The helper transmits the information at the second time slot, which is orthogonal to the first time slot.

There have been a volume of representative publications related to lossy cooperative wireless communications, which are summarized in Table I[2]. Among them, this paper specifically utilizes the landmark results of the fundamental limit analyses established by Wyner and Ziv [15].

Introduction is followed by information theoretic analyses, which is, however, *NOT the final goal of this paper but forms a mathematical basis for calculating the outage probability with the cooperative wireless IoT systems*. In fading wireless communication channels, the probability that the rate-distortion region, derived by the information theoretic analysis, can not be satisfied has to be averaged over the fading variations of the channels involved in the wireless network. Since the rate-distortion region is a function of the instantaneous signal-to-noise power ratios of the channels, the outage probability can be calculated by a multi-fold integral with respect to the probability density functions (PDFs) of the channel variations. Various results are introduced in a tutorial paper [28], where many results are based on Shannon's source-channel separation theorem [29], [30].

In Shannon's lossless source-channel separation theorem, the theoretical limit is achieved by an optimal multiterminal correlated source coding and the capacity-achieving channel codes [31], [32]. In the lossy case, the optimal multiterminal source coding compresses source sequences into codewords which satisfy the distortion requirement, and the source coding process is followed by capacity-achieving channel coding[3,4]. Therefore, the capacity-achieving channel codes can be regarded as the bridge that connects binary source information and channel coding using Gaussian codebooks. It should be noted that the source information should not necessarily be binary, but considering non-binary source sequence is out of the scope of this paper. To calculate the outage probability, this paper utilizes block fading assumption where the channel signal-to-noise ratios (SNRs) vary block-by-block, stay constant over each block. Then, the outage probability can be calculated as the probability that the rates supported by each channel's SNR fall outside the rate region for the successful transmission. As pointed out in [34, Section 14.1], the separate source-channel coding scheme for communications over MACs is not optimal in general but a sufficient condition, which can also be utilized for performance analyses over MACs such as [35], [36], and also as summarized in the tutorial paper [28].

There are also many achievements regarding outage probability analyses in fading channels besides the results shown in [28]. Im and Lee [37] derived a closed-form expression of the exact outage probability in a cooperative non-orthogonal multiple access (NOMA) system with imperfect successive interference cancellation. Liang *et al.* [38] investigated the outage probability of cooperative NOMA systems with imperfect channel state information in the high SNR regimes. Song *et al.* [36] analyzed the outage probability performance of Wyner-Ziv system over MACs and introduced a helper selection technique. Lin *et al.* [39] determined the outage probability for two correlated Gaussian sources transmitted through orthogonal Nakagami-m fading channels. Chen *et al.* [40] evaluated the outage probability of millimeter wave cellular systems assisted by a relay based on the joint spatial division and multiplexing. Qian *et al.* [41] characterized the outage probability of correlated information transmissions by NOMA with shadowed fading.

[1]With this structure, the recovery of the observation by Sensor 1 at the center is also assisted by the helper as shown by the red dashed line in the graphical abstract, because the observations by Sensors 1 and 2 are correlated.

[2]In this paper, both helper and side information represent that the information in the link does not need to be reconstructed. The difference is that helper has a rate constraint while side information has no rate constraint.

[3]Shannon's lossy source-channel theorem is understood as follows: the distortion caused by the errors due to transmission is equivalent to that caused by lossy compression before transmission and protected by channel coding yielding losless recovery of the compressed sequence. The analytical result derived from the theorem indicates only theoretical limit, however, it eliminates the necessity of utilizing the knowledge of channel state information.

[4]If the modulation type is specified, the channel capacity constraint should be given by the constellation constrained capacity (CCC) [33]. However, the analysis with CCC is out of the scope of this paper and left as future work.

TABLE I
REPRESENTATIVE PUBLICATIONS RELATED TO LOSSY COOPERATIVE WIRELESS COMMUNICATIONS

Literature	**With noiseless source ○ With noisy source only ×**	**With helper ○ With side information ● Without helper and side information ×**	**Finite set source ○ Binary source ◐ Gaussian source ●**
Lin *et al.* [10]	○	○	○
Lin and Matsumoto [11], [12]	○	○	○
Lin *et al.* [13]	○	○	◐
Oohama [14]	○	○	●
Wyner and Ziv [15]	○	●	○
Timo *et al.* [16]	○	●	○
Sechelea *et al.* [17]	○	●	◐
Berger [18]	○	×	○
Tung [19]	○	×	○
Shirani and Pradhan [20]	○	×	○
Xie *et al.* [21]	○	×	●
Yang and Xiong [22]	×	○	●
Oohama [23]–[25]	×	○	●
Schein and Gallager [26]	×	○	●

From the aforementioned literatures, we can identify that the problem, performance analysis of lossy cooperative wireless communications over MACs with a practical structure of helper, is worth being solved. Up to the authors' best knowledge, though, neither the achievable rate-distortion region nor the outage probability is analyzed for cooperative lossy communications with a bit-flipping (BF) helper, which can be also interpreted as a lossy-forward (LF) [28] helper. Hence, this paper aims at evaluating the rate-distortion and the outage probability performance of cooperative lossy communications with two sources and one BF helper over fading MAC. The contributions of this paper are summarized as follows:

- We establish an analytical framework for the rate-distortion and the outage probability analyses of cooperative lossy communications with a BF helper over the fading MAC.
- In the multiterminal source coding problem, we derive a closed-form expression of the inner bound on the achievable rate-distortion region with two sources and one BF helper. A joint Markov chain model is proposed for analyzing the effects of the correlations among the source information and the helper information.
- The outage probability of two-source-one-helper transmission over block Rayleigh or Nakagami-m fading MAC is approximately evaluated by utilizing a lower bound of the achievable rate-distortion. Specifically, the occurrence of outage events is categorized into three nominal cases, for which the outage probability of each case can accurately be evaluated by calculating the associated probabilities.
- We conduct a series of simulations to compare the outage probability performance between MAC and orthogonal transmissions, both suffering from block Rayleigh fading. The tendency of the approximated outage probability is also verified through the comparison between the simulation and numerical results.
- Moreover, we also make comparisons in terms of the outage probability between Rayleigh and Nakagami-m fading as well as between BF helper and optimal helper, to have performance tendency in different scenarios.

The remaining of this paper is organized as follows. Section II describes the mathematical system and channel models. Section III and Section IV derive the inner bound on the achievable rate-distortion region and the approximated outage probability, respectively. Then, the outage probability performance is evaluated by simulations and numerical integrals in Section V. Finally, Section VI contains some concluding statements.

The standard notation rules used throughout this paper are introduced as follows. The random variables and their realizations are denoted by uppercase and lowercase letters, respectively. Calligraphic letters denote the corresponding finite sets. The base of logarithm function $\log(\cdot)$ is assumed to be 2 unless specified.

II. PROBLEM FORMULATION

In this section, we formulate the system to be analyzed as a multiterminal source coding problem with two correlated sources and a BF helper. We then introduce the channel model to be used in the outage probability analysis.

A. System Model

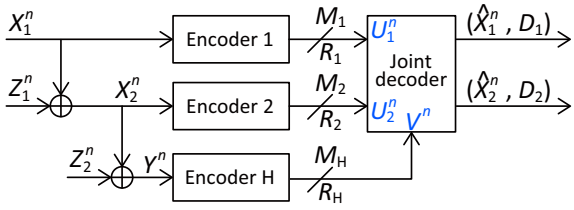

Fig. 1. The system model of cooperative communications with a BF helper.

Although the sensors and the helper transmit information at different time slots as depicted in the graphical abstract, the system only focuses on the whole round of transmissions for joint decoding. Hence, the whole round of transmissions can be formulated as a multiterminal source coding problem as illustrated in Fig. 1, with the source coding rates constraints of the channel capacities. There are two correlated discrete memoryless sources X_1 and X_2 jointly generating the information sequences $x_1^n = \{x_1(i)\}_{i=1}^n$ and $x_2^n = \{x_2(i)\}_{i=1}^n$, where i and n stand for the time index and the sequence length, respectively. At each time index i, the generated symbols $x_j(i)$ take values from the binary alphabet $\mathcal{X}_j = \{0, 1\}$ for $j = 1, 2$. If we separately describe two sources, each of them follows an independent and identically distributed (i.i.d.) Bernoulli distribution as $X_j \sim \text{Bern}(0.5)$ for $j = 1, 2$. However, X_1 and X_2 simultaneously have a crossover probability $\rho \in [0, 0.5]$. Hence, X_2 can be regarded as an output of a binary symmetric channel with the input X_1, i.e., $X_2 = X_1 \oplus Z_1$ with $Z_1 \sim \text{Bern}(\rho)$. Likewise, since the helper sequence y^n is the BF version of x_2^n, the helper information Y can be characterized by $Y = X_2 \oplus Z_2$ with $Z_2 \sim \text{Bern}(P_{e2})$, where P_{e2} represents the crossover probability between X_2 and Y.

At the transmitter side, the source sequences x_j^n and the helper sequence y^n are independently encoded by the encoder j and the encoder H with the coding rates R_j and R_{H}, respectively. The encoding process is described by mapping the input sequence onto a codeword index M with the following mapping rules:

$$\varphi_j : \mathcal{X}_j^n \mapsto \mathcal{M}_j = \{1, 2, \cdots, 2^{nR_j}\}, \text{ for } j = 1, 2, \quad (1)$$

$$\varphi_{\text{H}} : \mathcal{Y}^n \mapsto \mathcal{M}_{\text{H}} = \{1, 2, \cdots, 2^{nR_{\text{H}}}\}, \quad (2)$$

where $\mathcal{X}_j^n$ and $\mathcal{Y}^n$ represent the n-fold alphabets of the source sequences and the helper sequence, respectively. Correspondingly, $\mathcal{M}_j$ and $\mathcal{M}_{\text{H}}$ denote the codeword sets in each link.

After receiving all the codeword indices $\varphi_1(x_1^n)$, $\varphi_2(x_2^n)$ and $\varphi_{\text{H}}(y^n)$, the decoder jointly reconstructs the source sequences by the following mapping

$$\psi : \mathcal{M}_1 \times \mathcal{M}_2 \times \mathcal{M}_{\text{H}} \mapsto \mathcal{X}_1^n \times \mathcal{X}_2^n. \quad (3)$$

U_j^n and V^n represent the compressed version of X_j^n and Y^n, respectively. The recovered sequences $\hat{x}_1^n$ and $\hat{x}_2^n$ may deviate from the original sequences x_1^n and x_2^n due to insufficient coding rates. To evaluate the distortion in the recovered sequences, the Hamming distortion measure is adopted as

$$d_j(x_j, \hat{x}_j) = \begin{cases} 1, & \text{if } x_j \neq \hat{x}_j, \\ 0, & \text{if } x_j = \hat{x}_j, \end{cases} \text{ for } j = 1, 2. \quad (4)$$

For the entire sequence, the average distortion between the sequences x_j^n and $\hat{x}_j^n$ is defined as

$$d_j(x_j^n, \hat{x}_j^n) = \frac{1}{n} \sum_{i=1}^{n} d_j(x_j(i), \hat{x}_j(i)), \text{ for } j = 1, 2. \quad (5)$$

Finally, the achievable rate-distortion region satisfying the specified distortion requirements (D_1, D_2) is defined as

$$\begin{aligned} &\mathcal{R}(D_1, D_2) \\ &= \big\{(R_1, R_2, R_{\text{H}}) : (R_1, R_2, R_{\text{H}}) \text{ is achievable such that} \\ &\qquad \lim_{n\to\infty} \text{E}(d_j(x_j^n, \hat{x}_j^n)) \leq D_j + \epsilon, \\ &\qquad \text{for } j = 1, 2, \text{ and any } \epsilon > 0\big\}. \end{aligned} \quad (6)$$

B. Channel Model

We assume that two source links are modeled by block Rayleigh or Nakagami-m fading channels. Specifically, the complex channel gains in each source link independently follows the two-dimensional Gaussian distribution frame by frame, while the channel fading keeps constant in the same frame. Hence, the PDF of the instantaneous SNR in each source link is given by

$$p(\gamma_j) = \frac{1}{\overline{\gamma}_j} \exp\left(-\frac{\gamma_j}{\overline{\gamma}_j}\right), \text{ for } j = 1, 2, \quad (7)$$

where γ_j and $\overline{\gamma}_j$ stand for the instantaneous SNR and the average SNR, respectively.

For Nakagami-m fading, the PDF of the instantaneous SNR follows the Gamma distribution, given by

$$p(\gamma_j) = \frac{m^m \gamma_j^{m-1}}{\overline{\gamma}_j^m \Gamma(m)} \exp\left(-\frac{m\gamma_j}{\overline{\gamma}_j}\right), \text{ for } j = 1, 2, \quad (8)$$

where $\Gamma(\cdot)$ represents the Gamma function [42, Eq. (4-35)]. It is obvious that when $m = 1$, (8) is equal to (7), i.e., the Nakagami-m fading reduces to the Rayleigh fading.

In practical scenarios, the channel gain of the helper link could be either stochastic or static, e.g., the helper transmits information through wired link. Since this paper only focuses on the performance effect of MAC, we adopt the assumption of the static helper link for simplicity.

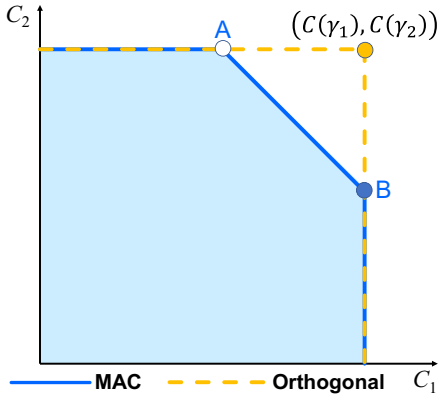

Fig. 2. The achievable capacity region for MAC and orthogonal channels.

For the transmissions of X_1 and X_2 over orthogonal channels, the channel capacity for each channel is $C_j \triangleq C(\gamma_j)$ for $j = 1, 2$, where $C(\gamma_j) = \log(1 + \gamma_j)$ represents the Shannon capacity for two-dimensional signalling using Gaussian codebook. When X_1 and X_2 are transmitted over MAC, the achievable region of the channel capacities is illustrated in

Fig. 2 [34, Figure 4.7]. The corresponding capacity pairs for two corner points A and B are [34, Theorem 4.4]

$$\begin{cases} C_{A1} = C\left(\dfrac{\gamma_1}{1+\gamma_2}\right), \\ C_{A2} = C(\gamma_2), \end{cases} \tag{9}$$

and

$$\begin{cases} C_{B1} = C(\gamma_1), \\ C_{B2} = C\left(\dfrac{\gamma_2}{1+\gamma_1}\right). \end{cases} \tag{10}$$

Thus, it is easy to find that the decay of the line AB is -1.

III. Rate-Distortion Analysis

A. Derivation of Rate-Distortion Functions

For the system with two sources and one helper, the inner bound on the achievable rate-distortion region is [11]

$$R_1 > I(X_1; U_1|U_2, V, Q), \tag{11}$$
$$R_2 > I(X_2; U_2|U_1, V, Q), \tag{12}$$
$$R_1 + R_2 > I(X_1, X_2; U_1, U_2|V, Q), \tag{13}$$
$$R_{\mathrm{H}} > I(Y; V), \tag{14}$$

for some conditional probability mass function $p(q)p(u_1|x_1, q)$ $p(u_2|x_2, q)p(v|y)$, where Q is an auxiliary variable resulting from the time-sharing scheme [34, Section 4.4], and takes value from a set $\mathcal{Q}$. Moreover, $U_2 \to X_2 \to X_1 \to U_1$ and $V \to Y \to (X_1, X_2) \to (U_1, U_2)$ form Markov chains. The rate-distortion region given by the inner bound can be exactly achieved by the distributed compress-bin scheme [34, Chapter 12] for joint source coding.

Now, we calculate the inner bound on the achievable rate-distortion region for a BF helper with $|\mathcal{Q}| = 1$, and the results can be extended to general cases by the time-sharing scheme. First, consider

$$\begin{aligned} R_1 &> I(X_1; U_1|U_2, V) \\ &= H(U_1|U_2, V) - H(U_1|X_1, U_2, V) \\ &= H(U_1|U_2, V) - H(U_1|X_1) \qquad (15) \\ &= H(U_1, U_2|V) - H(U_2|V) - H(U_1|X_1), \qquad (16) \end{aligned}$$

where (15) follows $V \to X_1 \to U_1$ and $U_2 \to X_1 \to U_1$ forming two Markov chains.

Then, similarly to the calculation of R_1, we obtain

$$R_2 > H(U_1, U_2|V) - H(U_1|V) - H(U_2|X_2). \tag{17}$$

Next, consider

$$\begin{aligned} R_1 + R_2 &> I(X_1, X_2; U_1, U_2|V) \\ &= H(U_1, U_2|V) - H(U_1, U_2|X_1, X_2, V) \\ &= H(U_1, U_2|V) - H(U_1, U_2|X_1, X_2) \qquad (18) \\ &= H(U_1, U_2|V) - H(U_1|X_1, X_2) \\ &\quad - H(U_2|X_1, X_2, U_1) \\ &= H(U_1, U_2|V) - H(U_1|X_1) - H(U_2|X_2), \qquad (19) \end{aligned}$$

where (18) follows since $V \to Y \to (X_1, X_2) \to (U_1, U_2)$ form a Markov chain, and (19) follows since $X_2 \to X_1 \to U_1$ and $U_1 \to X_1 \to X_2 \to U_2$ form two Markov chains.

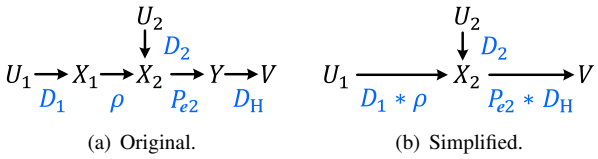

(a) Original. (b) Simplified.

Fig. 3. joint Markov chains for rate-distortion analysis.

To further calculate (16), (17) and (19), we need to calculate $H(U_1, U_2|V)$, $H(U_j|V)$ and $H(U_j|X_j)$ for $j = 1, 2$. For the calculations of $H(U_j|V)$ and $H(U_j|X_j)$, we rely on the joint Markov chains illustrated in Fig. 3(a), which represents the information transition and the corresponding crossover probability. To calculate $H(U_1, U_2|V)$, the joint Markov chains are equivalently simplified into Fig. 3(b). To simplify expressions, we denote $\rho_1 = D_1 * \rho$, $\rho_2 = D_2$, and $\rho_V = P_{e2} * D_{\mathrm{H}}$, respectively, where the operator $*$ represents the binary convolution, i.e., $a * b = a(1-b) + b(1-a)$. In addition, we write $D_{\mathrm{H}} = H_b^{-1}(1 - R_{\mathrm{H}})$ where $H_b^{-1}(\cdot)$ denotes the inverse function of the binary entropy function $H_b(p) = -p\log p - (1-p)\log(1-p)$.

It should be noticed that with the joint Markov chain, X_2 is reconstructed from U_2, while the effectiveness of V is only to reduce R_2 by providing a certain part of the mutual information between X_2 and U_2. There exists probability that V partially contains information of X_2 which does not belongs to the mutual information between X_2 and U_2. Hence, the joint Markov chain structure may require excessive rate due to not utilizing the information provided by V, resulting in the specifically calculated rate-distortion region to be an upper bound.

From Fig. 3, we have

$$H(U_j|V) = H_b(\rho_j * \rho_V), \tag{20}$$
$$H(U_j|X_j) = H_b(D_j). \tag{21}$$

For the calculation of $H(U_1, U_2|V)$, we need to use the definition of joint conditional entropy, i.e.,

$$H(U_1, U_2|V) = -\sum_{u_1, u_2, v} p(u_1, u_2, v)\log p(u_1, u_2|v). \tag{22}$$

Since $p(u_1, u_2, v) = p(u_1, u_2|v)p(v)$, the key to calculating $H(U_1, U_2|V)$ is to obtain the joint conditional probability $p(u_1, u_2|v)$. For the calculation of $p(u_1, u_2|v)$, we need to analyze the transition probabilities of the simplified joint Markov chains depicted in Fig. 3(b).

Note that X_2 is the common variable in the joint Markov chain. Therefore, the information transition from different variables is coupled by X_2. For example, if the transition of $u_1 \to x_2$ with $x_2 = 0$ occurs, then u_1 has to transfer to 0 too in the transition of $u_1 \to x_2$. For a specified value of x_2, we can obtain the coupling cases for u_1 and u_2 and their corresponding probabilities as listed in Table II. Then, by assigning specified values to v, u_1 and u_2, the joint conditional probability $p(u_1, u_2|v)$ is derived in Table III.

It is easy to find that the case of $v = 1$ is symmetric to the

TABLE II
TRANSITION PROBABILITIES OF JOINT MARKOV CHAINS

Case	Probability	Coupling case	Probability
$x_2 = v$	$1-\rho_V$	$u_1 = v$	$1-\rho_1$
		$u_1 \neq v$	ρ_1
		$u_2 = v$	$1-\rho_2$
		$u_2 \neq v$	ρ_2
$x_2 \neq v$	ρ_V	$u_1 = v$	ρ_1
		$u_1 \neq v$	$1-\rho_1$
		$u_2 = v$	ρ_2
		$u_2 \neq v$	$1-\rho_2$

TABLE III
JOINT CONDITIONAL PROBABILITY $p(u_1, u_2|v)$

v	u_1, u_2	$p(u_1, u_2|v)$
0	0, 0	$\rho_1\rho_2\rho_V + (1-\rho_1)(1-\rho_2)(1-\rho_V)$
	0, 1	$\rho_1(1-\rho_2)\rho_V + (1-\rho_1)\rho_2(1-\rho_V)$
	1, 0	$(1-\rho_1)\rho_2\rho_V + \rho_1(1-\rho_2)(1-\rho_V)$
	1, 1	$\rho_1\rho_2(1-\rho_V) + (1-\rho_1)(1-\rho_2)\rho_V$
1	1, 1	$\rho_1\rho_2\rho_V + (1-\rho_1)(1-\rho_2)(1-\rho_V)$
	1, 0	$\rho_1(1-\rho_2)\rho_V + (1-\rho_1)\rho_2(1-\rho_V)$
	0, 1	$(1-\rho_1)\rho_2\rho_V + \rho_1(1-\rho_2)(1-\rho_V)$
	0, 0	$\rho_1\rho_2(1-\rho_V) + (1-\rho_1)(1-\rho_2)\rho_V$

case of $v = 0$. Hence, we can calculate $H(U_1, U_2|V)$ as

$$\begin{aligned} H(U_1,U_2|V) &= -\sum_{u_1,u_2,v} p(u_1,u_2,v)\log p(u_1,u_2|v) \\ &= -\sum_{u_1,u_2} p(u_1,u_2,0)\log p(u_1,u_2|0) \\ &\quad -\sum_{u_1,u_2} p(u_1,u_2,1)\log p(u_1,u_2|1) \\ &= -2\sum_{u_1,u_2} p(u_1,u_2,0)\log p(u_1,u_2|0) \\ &= -2\sum_{u_1,u_2} p(u_1,u_2|0)p(v=0)\log p(u_1,u_2|0) \\ &= -2\sum_{u_1,u_2} p(u_1,u_2|0)\cdot\frac{1}{2}\cdot\log p(u_1,u_2|0) \\ &= -\sum_{u_1,u_2} p(u_1,u_2|0)\log p(u_1,u_2|0). \end{aligned} \tag{23}$$

By substituting the joint conditional probability listed in Table III into (23), we can calculate the exact value of $H(U_1, U_2|V)$.

Now, by calculation of $H(U_1, U_2|V)$, $H(U_j|V)$ and $H(U_j|X_j)$ for $j = 1, 2$, the inner bound on the achievable rate-distortion region is obtained as

$$R_1 > H(U_1,U_2|V) - H_b(\rho_2 * \rho_V) - H_b(D_1), \tag{24}$$
$$R_2 > H(U_1,U_2|V) - H_b(\rho_1 * \rho_V) - H_b(D_2), \tag{25}$$
$$R_1 + R_2 > H(U_1,U_2|V) - H_b(D_1) - H_b(D_2), \tag{26}$$

where $H(U_1, U_2|V)$ is calculated by (23).

B. Rate-Distortion Region

Based on the results of (24)–(26) for $|\mathcal{Q}| = 1$, we are able to plot the achievable rate-distortion region by time-sharing scheme. Specifically, we now describe the three cases for which the rate pair (R_1, R_2) falls on the boundary of the achievable rate-distortion region.

Case 1: R_1 be sufficiently large to satisfy D_1 without the help of U_2. Hence, the exact distortion for the recovery of $\hat{X}_1$ can be $\tilde{d}_1 \leq D_1$. In this case, the compressed information U_1 provides the side information for the joint decoder to reconstruct $\hat{X}_2$, i.e., X_1 can be equivalently regarded as a helper. Furthermore, since (R_1, R_2) is on the boundary of the achievable rate-distortion region, the distortion of $\hat{X}_2$ has to be D_2. For the decoding of $\hat{X}_1$ without the help of U_2, we have

$$\begin{aligned} R_1 &= I(X_1;U_1|V) \\ &= H(U_1|V) - H(U_1|X_1,V) \\ &= H(U_1|V) - H(U_1|X_1) \qquad (27) \\ &= H_b(\tilde{\rho}_1 * \rho_V) - H_b(\tilde{d}_1), \qquad (28) \end{aligned}$$

where (27) follows since $V \to X_1 \to U_1$ forms a Markov chain, and $\tilde{\rho}_1 = \tilde{d}_1 * \rho$.

For the joint decoding of $\hat{X}_2$ with the help of U_1 and V, we have

$$R_2 = H(U_1,U_2|V) - H_b(\tilde{\rho}_1 * \rho_V) - H_b(D_2). \tag{29}$$

Consequently, by assigning a value in $[0, D_1]$ to $\tilde{d}_1$, we can obtain a rate pair (R_1, R_2) on the boundary of the achievable rate-distortion region from (28) and (29). In addition, note that $D_1 = 0$ can be satisfied for any $R_1 \geq H_b(\tilde{\rho}_1 * \rho_V) - H_b(\tilde{d}_1)$ with $\tilde{d}_1 = 0$. Therefore, the complete boundary of the achievable rate-distortion region for Case 1 is

$$\begin{cases} R_1 > H_b(\tilde{\rho}_1 * \rho_V) - H_b(\tilde{d}_1), & \text{for } \tilde{d}_1 = 0, \\ R_1 = H_b(\tilde{\rho}_1 * \rho_V) - H_b(\tilde{d}_1), & \text{for } 0 < \tilde{d}_1 \leq D_1, \end{cases} \tag{30}$$

and

$$R_2 = H(U_1,U_2|V) - H_b(\tilde{\rho}_1 * \rho_V) - H_b(D_2), \quad \text{for } 0 \leq \tilde{d}_1 \leq D_1. \tag{31}$$

Case 2: In a similar way to Case 1, when R_2 is sufficiently large to satisfy D_2 without the help of U_1, the exact distortion for the recovery of $\hat{X}_2$ is $\tilde{d}_2 \leq D_2$. Hence, we have

$$\begin{cases} R_2 > H_b(\tilde{\rho}_2 * \rho_V) - H_b(\tilde{d}_2), & \text{for } \tilde{d}_2 = 0, \\ R_2 = H_b(\tilde{\rho}_2 * \rho_V) - H_b(\tilde{d}_2), & \text{for } 0 < \tilde{d}_2 \leq D_2, \end{cases} \tag{32}$$

and

$$R_1 = H(U_1,U_2|V) - H_b(\tilde{\rho}_2 * \rho_V) - H_b(D_1), \quad \text{for } 0 \leq \tilde{d}_2 \leq D_2, \tag{33}$$

with $\tilde{\rho}_2 = \tilde{d}_2$.

Case 3: Neither R_1 nor R_2 is sufficiently large to satisfy its own distortion requirement without the help of each other. In this case, $\hat{X}_1$ and $\hat{X}_2$ achieve the minimum distortions D_1 and D_2 by joint decoding. Consider the extreme value $\tilde{d}_1 = D_1$ in Case 1, and hence the following rate pair is achievable:

$$\begin{cases} R_1 = H_b(\rho_1 * \rho_V) - H_b(D_1), \\ R_2 = H(U_1,U_2|V) - H_b(\rho_1 * \rho_V) - H_b(D_2). \end{cases} \tag{34}$$

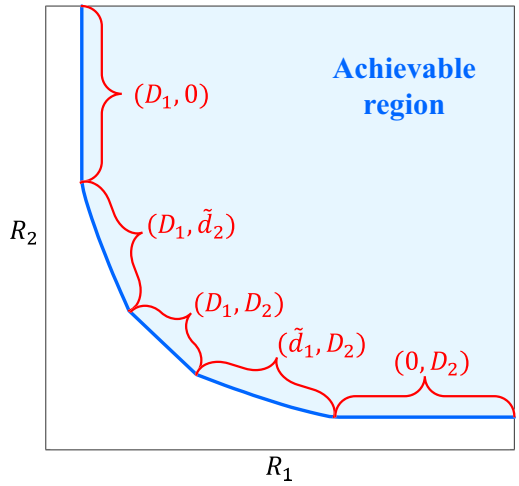

Fig. 4. The inner bound on the achievable rate-distortion region.

Likewise, for the extreme value $\tilde{d}_2 = D_2$ in Case 2, the following rate pair is achievable:

$$\begin{cases} R_1 = H(U_1, U_2|V) - H_b(\rho_2 * \rho_V) - H_b(D_1), \\ R_2 = H_b(\rho_2 * \rho_V) - H_b(D_2). \end{cases} \tag{35}$$

Since both the corner points given by (34) and (35) satisfy the distortions (D_1, D_2), the rate pairs on the line connecting these two corner points also satisfy the distortions (D_1, D_2) based on the time-sharing scheme. Hence, when the distortions of $\hat{X}_1$ and $\hat{X}_2$ are, respectively, D_1 and D_2, the rate pair should satisfy

$$R_1 + R_2 = H(U_1, U_2|V) - H_b(D_1) - H_b(D_2), \tag{36}$$

$$R_1 \le H_b(\rho_1 * \rho_V) - H_b(D_1), \tag{37}$$

$$R_2 \le H_b(\rho_2 * \rho_V) - H_b(D_2). \tag{38}$$

By combining the aforementioned three cases, we can depict the achievable rate-distortion region as Fig. 4, whose boundary consists of two curves and three straight lines. In addition, the corresponding distortions are marked in each curve or straight line.

IV. Outage Probability Analysis

A. Outage Probability in Rayleigh Fading

According to the lossy source-channel separation theorem [29], [30], the distortion requirements (D_1, D_2) can be satisfied if

$$R_j(D_j) \le \Theta_j(\gamma_j) = \frac{C(\gamma_j)}{r_j}, \text{ for } j = 1, 2, \tag{39}$$

where r_j denotes the end-to-end coding rate. Here, r_j can be regarded as a coefficient for scaling the coding rate from the channel coding domain to the source coding domain.

Then, the achievable region of the channel capacities in Fig. 2 can be mapped from the channel coding domain to the source coding domain as Fig. 5. Therefore, the two corner points in the achievable rate region over MAC become

$$\begin{cases} R_{A1} = \Theta_1\left(\dfrac{\gamma_1}{1+\gamma_2}\right), \\ R_{A2} = \Theta_2(\gamma_2), \end{cases} \tag{40}$$

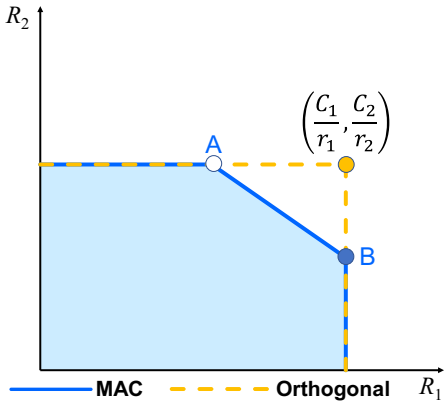

Fig. 5. The achievable rate region for MAC and orthogonal channels.

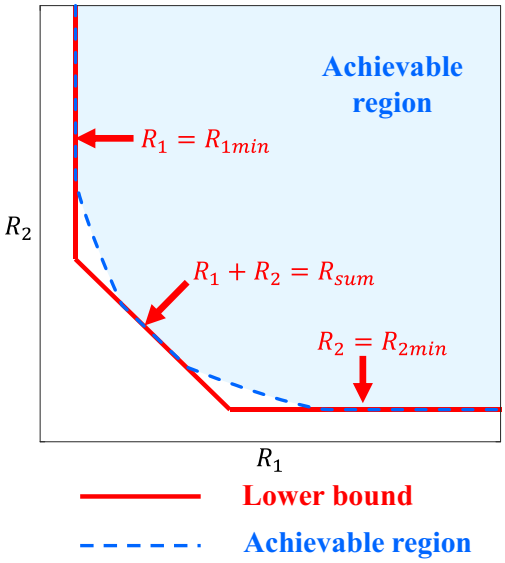

Fig. 6. The lower bound of the achievable rate-distortion region for approximation.

and

$$\begin{cases} R_{B1} = \Theta_1(\gamma_1), \\ R_{B2} = \Theta_2\left(\dfrac{\gamma_2}{1+\gamma_1}\right). \end{cases} \tag{41}$$

Note that when mapping the achievable MAC region from the channel coding domain to the source coding domain, the region is, respectively, scaled by r_1 and r_2 in the horizontal and the vertical directions over the axes of the achievable rate pairs. Hence, the gradient of the line AB is not equal to -1 in the source coding domain, unless $r_1 = r_2$.

In the source coding domain, if the MAC region and the rate-distortion region overlap, it means that the channel conditions can support the transmission rates which satisfy the distortion requirements. Otherwise, the distortions exceed the requirements and an outage event occurs.

Since the achievable rate-distortion region has a complicated shape, the calculation of the outage probability is also intricate. To simplify the calculation of the outage probability, we make an approximation of the achievable rate-distortion region as illustrated in Fig. 6. The achievable rate-distortion region is

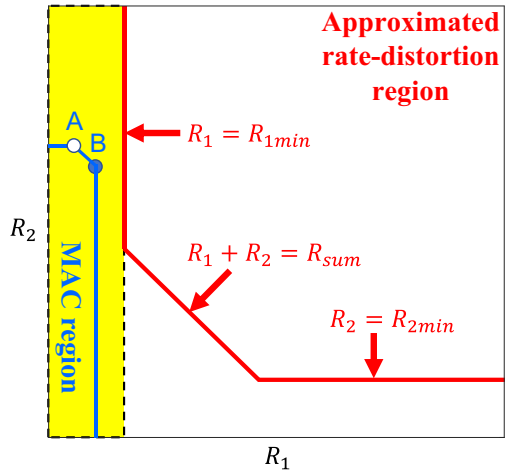

Fig. 7. Outage case 1 for calculating the outage probability.

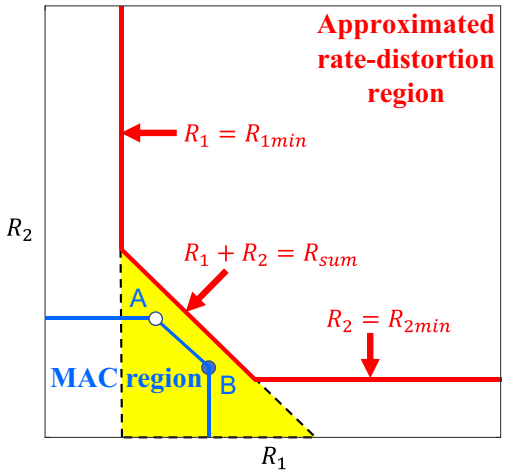

Fig. 8. Outage case 2 for calculating the outage probability.

approximated by a lower bound consisting of three straight lines[5]:

$$R_1 = R_{1\min}, \tag{42}$$
$$R_2 = R_{2\min}, \tag{43}$$
$$R_1 + R_2 = R_{\text{sum}}, \tag{44}$$

where

$$R_{1\min} = H(U_1, U_2|V) - H_b(\tilde{\rho}_2 * \rho_V) - H_b(D_1), \tag{45}$$
$$R_{2\min} = H(U_1, U_2|V) - H_b(\tilde{\rho}_1 * \rho_V) - H_b(D_2), \tag{46}$$
$$R_{\text{sum}} = H(U_1, U_2|V) - H_b(D_1) - H_b(D_2), \tag{47}$$

with $\tilde{d}_1 = \tilde{d}_2 = 0$. Then, the cases of outage events can be classified as follows.

Outage Case 1: As shown in Fig. 7, the corner point B falls in the region of

$$0 \le R_1 < R_{1\min}, \tag{48}$$
$$0 \le R_2 < \infty. \tag{49}$$

In this case, the MAC region cannot overlap with the rate-distortion region, wherever the corner point A is. Hence, the probability for this case is

$$\begin{aligned} P_1 &= \Pr\{0 \le R_{B1} < R_{1\min}\} \\ &= \Pr\{0 \le \Theta_1(\gamma_1) < R_{1\min}\} \\ &= \Pr\{\Theta_1^{-1}(0) \le \gamma_1 < \Theta_1^{-1}(R_{1\min})\} \\ &= \int_0^{\Theta_1^{-1}(R_{1\min})} p(\gamma_1) d\gamma_1 \qquad (50) \\ &= 1 - \exp\left[-\frac{\Theta_1^{-1}(R_{1\min})}{\overline{\gamma}_1}\right], \qquad (51) \end{aligned}$$

where $\Theta_j^{-1}(\cdot)$ is the inverse function of $\Theta_j(\cdot)$.

[5]By this means, it is very simple to get the straight line equations with a sufficient level of accuracy, as this will be confirmed by numerical simulations in Section V-B.

Outage Case 2: As depicted in Fig. 7, the corner point B falls in the region of

$$R_{1\min} \le R_1, \tag{52}$$
$$0 \le R_2, \tag{53}$$
$$R_1 + R_2 < R_{\text{sum}}. \tag{54}$$

If $r_1 \neq r_2$, the gradient of the line AB is not equal to -1 as discussed in Fig. 5. Then, the line AB is not parallel to the line of $R_1 + R_2 = R_{\text{sum}}$, resulting in complicated subcases for the occurrence of the outage events. In the real world, it is common that two links have the same end-to-end coding rate, i.e., $r_1 = r_2$. In the case of $r_1 = r_2$, the line AB is parallel to the line of $R_1 + R_2 = R_{\text{sum}}$, and hence the MAC region cannot overlap with the rate-distortion region regardless of the position of the corner point A. Thus, the probability for this case is given by

$$\begin{aligned} P_2 &= \Pr\{R_{1\min} \le R_{B1}, 0 \le R_{B2}, R_{B1} + R_{B2} < R_{\text{sum}}\} \\ &= \Pr\{R_{1\min} \le R_{B1} < R_{\text{sum}}, R_{B2} < R_{\text{sum}} - R_{B1}\} \\ &= \Pr\Bigg\{R_{1\min} \le \Theta_1(\gamma_1) < R_{\text{sum}}, \\ &\qquad \Theta_2\left(\frac{\gamma_2}{1+\gamma_1}\right) < R_{\text{sum}} - \Theta_1(\gamma_1)\Bigg\} \\ &= \Pr\{\Theta_1^{-1}(R_{1\min}) \le \gamma_1 < \Theta_1^{-1}(R_{\text{sum}}), \\ &\qquad \gamma_2 < (1+\gamma_1)\Theta_2^{-1}[R_{\text{sum}} - \Theta_1(\gamma_1)]\} \\ &= \int_{\Theta_1^{-1}(R_{1\min})}^{\Theta_1^{-1}(R_{\text{sum}})} d\gamma_1 \int_0^{\xi(\gamma_1)} p(\gamma_1)p(\gamma_2)d\gamma_2 \qquad (55) \\ &= \int_{\Theta_1^{-1}(R_{1\min})}^{\Theta_1^{-1}(R_{\text{sum}})} \frac{1}{\overline{\gamma}_1} \exp\left(-\frac{\gamma_1}{\overline{\gamma}_1}\right) \\ &\qquad \cdot \left[1 - \exp\left(-\frac{\xi(\gamma_1)}{\overline{\gamma}_2}\right)\right] d\gamma_1, \qquad (56) \end{aligned}$$

where $\xi(\gamma_1) = (1+\gamma_1)\Theta_2^{-1}[R_{\text{sum}} - \Theta_1(\gamma_1)]$. Although it is difficult to further obtain a closed-form expression of P_2, we can numerically calculate (56).

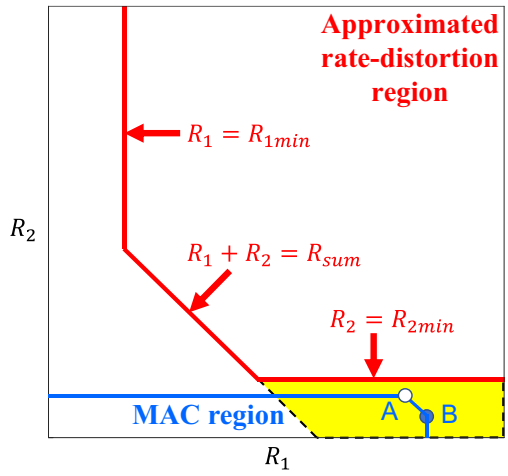

Fig. 9. Outage case 3 for calculating the outage probability.

Outage Case 3: As presented in Fig. 9, the corner point B falls in the region of

$$0 \le R_2 < R_{2\min}, \tag{57}$$
$$R_{\text{sum}} \le R_1 + R_2. \tag{58}$$

Meanwhile, the corner point A should also be under the line of $R_2 = R_{2\min}$, i.e., $R_{A2} < R_{2\min}$. Therefore, the probability in this case can be expressed as

$$\begin{aligned} P_3 &= \Pr\{0 \le R_{B2} < R_{2\min}, R_{\text{sum}} \le R_{B1} + R_{B2}, \\ &\qquad R_{A2} < R_{2\min}\} \\ &= \Pr\left\{0 \le \Theta_2\left(\frac{\gamma_2}{1+\gamma_1}\right) < R_{2\min}, \right. \\ &\qquad R_{\text{sum}} \le \Theta_1(\gamma_1) + \Theta_2\left(\frac{\gamma_2}{1+\gamma_1}\right), \\ &\qquad \left.\Theta_2(\gamma_2) < R_{2\min}\right\} \\ &= \Pr\left\{0 \le \gamma_2 < (1+\gamma_1)\Theta_2^{-1}(R_{2\min}), \right. \\ &\qquad R_{\text{sum}} \le \Theta_1(\gamma_1) + \Theta_2\left(\frac{\gamma_2}{1+\gamma_1}\right), \\ &\qquad \left.\gamma_2 < \Theta_2^{-1}(R_{2\min})\right\} \\ &= \Pr\left\{0 \le \gamma_2 < \Theta_2^{-1}(R_{2\min}), \right. \\ &\qquad \left. R_{\text{sum}} \le \Theta_1(\gamma_1) + \Theta_2\left(\frac{\gamma_2}{1+\gamma_1}\right)\right\}. \end{aligned} \tag{59}$$

For the second constraint in (59), we have

$$\begin{aligned} R_{\text{sum}} &\le \Theta_1(\gamma_1) + \Theta_2\left(\frac{\gamma_2}{1+\gamma_1}\right) \\ &= \frac{1}{r_1}\log(1+\gamma_1) + \frac{1}{r_2}\log\left(1+\frac{\gamma_2}{1+\gamma_1}\right) \\ &= \frac{1}{r_1 r_2}\left[\log(1+\gamma_1)^{r_2} + \log\left(1+\frac{\gamma_2}{1+\gamma_1}\right)^{r_1}\right] \\ &= \frac{1}{r_1 r_2}\log\left[(1+\gamma_1)^{r_2-r_1}(1+\gamma_1+\gamma_2)^{r_1}\right]. \end{aligned} \tag{60}$$

Notice that it is not easy to obtain a closed-form expression of the constraint on γ_1 from (60) if $r_1 \ne r_2$. One feasible solution for calculating R_{sum} is applying numerical methods for calculation of γ_1. Conversely, a closed-form solution is easily calculated when $r_1 = r_2$. Under the practical assumption of $r_1 = r_2$, we have

$$\begin{aligned} R_{\text{sum}} &\le \frac{1}{r_2}\log(1+\gamma_1+\gamma_2) \\ &= \Theta_2(\gamma_1+\gamma_2), \end{aligned} \tag{61}$$

and hence

$$\Theta_2^{-1}(R_{\text{sum}}) - \gamma_2 \le \gamma_1, \text{ for } r_1 = r_2. \tag{62}$$

Now, (59) can be further calculated as

$$\begin{aligned} P_3 &= \Pr\{0 \le \gamma_2 < \Theta_2^{-1}(R_{2\min}), \Theta_2^{-1}(R_{\text{sum}}) - \gamma_2 \le \gamma_1\} \\ &= \int_0^{\Theta_2^{-1}(R_{2\min})} d\gamma_2 \int_{\Theta_2^{-1}(R_{\text{sum}})-\gamma_2}^{\infty} p(\gamma_1)p(\gamma_2)d\gamma_1 \qquad (63) \\ &= \int_0^{\Theta_2^{-1}(R_{2\min})} \frac{1}{\overline{\gamma}_2}\exp\left[-\frac{\gamma_2}{\overline{\gamma}_2} - \frac{\Theta_2^{-1}(R_{\text{sum}})-\gamma_2}{\overline{\gamma}_1}\right] d\gamma_2. \qquad (64) \end{aligned}$$

Finally, similar to the previous works [10], [13], [36], [43], we can numerically calculate the integrals to obtain the total outage probability by

$$P_{\text{out}} = P_1 + P_2 + P_3. \tag{65}$$

B. Outage Probability in Nakagami-m Fading

For Nakagami-m fading, we can calculate P_1 from (50) as

$$\begin{aligned} P_1 &= \int_0^{\Theta_1^{-1}(R_{1\min})} \frac{m^m \gamma_1^{m-1}}{\overline{\gamma}_1^m \Gamma(m)} \exp\left(-\frac{m\gamma_1}{\overline{\gamma}_1}\right) d\gamma_1 \\ &= 1 - \frac{\Gamma\left(m, \frac{m\Theta_1^{-1}(R_{1\min})}{\overline{\gamma}_1}\right)}{\Gamma(m)}, \end{aligned} \tag{66}$$

where $\Gamma(\cdot,\cdot)$ stands for the upper incomplete gamma function, and (66) follows according to [44, Eq. (3.381.3)].

For P_2, we can calculate from (55) as

$$\begin{aligned} P_2 &= \int_{\Theta_1^{-1}(R_{1\min})}^{\Theta_1^{-1}(R_{\text{sum}})} \frac{m^m \gamma_1^{m-1}}{\overline{\gamma}_1^m \Gamma(m)} \exp\left(-\frac{m\gamma_1}{\overline{\gamma}_1}\right) d\gamma_1 \\ &\quad \cdot \int_0^{\xi(\gamma_1)} \frac{m^m \gamma_2^{m-1}}{\overline{\gamma}_2^m \Gamma(m)} \exp\left(-\frac{m\gamma_2}{\overline{\gamma}_2}\right) d\gamma_2 \\ &= \int_{\Theta_1^{-1}(R_{1\min})}^{\Theta_1^{-1}(R_{\text{sum}})} \frac{m^m \gamma_1^{m-1}}{\overline{\gamma}_1^m \Gamma(m)} \exp\left(-\frac{m\gamma_1}{\overline{\gamma}_1}\right) \\ &\quad \cdot \left[1 - \frac{\Gamma\left(m, \frac{m\xi(\gamma_1)}{\overline{\gamma}_2}\right)}{\Gamma(m)}\right] d\gamma_1. \end{aligned} \tag{67}$$

For P_3, we can calculate from (63) as

$$P_3 = \int_0^{\Theta_2^{-1}(R_{2\min})} \frac{m^m \gamma_2^{m-1}}{\overline{\gamma}_2^m \Gamma(m)} \exp\left(-\frac{m\gamma_2}{\overline{\gamma}_2}\right) d\gamma_2 \cdot \int_{\Theta_2^{-1}(R_{\text{sum}})-\gamma_2}^{\infty} \frac{m^m \gamma_1^{m-1}}{\overline{\gamma}_1^m \Gamma(m)} \exp\left(-\frac{m\gamma_1}{\overline{\gamma}_1}\right) d\gamma_1$$
$$= \int_0^{\Theta_2^{-1}(R_{2\min})} \frac{m^m \gamma_2^{m-1}}{\overline{\gamma}_2^m [\Gamma(m)]^2} \exp\left(-\frac{m\gamma_2}{\overline{\gamma}_2}\right) \cdot \Gamma\left(m, \frac{m\left[\Theta_2^{-1}(R_{\text{sum}}) - \gamma_2\right]}{\overline{\gamma}_1}\right) d\gamma_2. \quad (68)$$

Since the upper incomplete gamma function $\Gamma(\cdot,\cdot)$ in (67) and (68) is represented in an integral form, deriving a closed-form expression for an integral having integrand $\Gamma(\cdot,\cdot)$ is of intractable difficulty. By substituting (66)-(68) into (65) and utilizing numerical methods, we can obtain the lower bound of the outage probability under Nakagami-m fading.

V. Performance Evaluation

This section evaluates and compares the system performance represented by the outage probability through Monte-Carlo methods [45] and numerical integrals. Such results are useful to guide the design of a practical coding scheme. The Monte-Carlo method generates instantaneous SNR following the channel models in (7), and then evaluates the probability that the generated rate tuple supported by the channel capacities falls outside the achievable rate-distortion region. For the identification of the cases resulting in outage with MAC, we need to calculate the two corner points A and B in the coordinate from the generated instantaneous SNRs with the links. Then, we judge the following three conditions step by step: 1) the sum rate is less than R_{sum}; 2) both points A and B have insufficient R_1; 3) both points A and B have insufficient R_2. If any step of condition is satisfied, an outage event occurs and we stop judging the remaining steps of conditions, because in such cases, no intersection between MAC region and rate-distortion region happens. If none of the three conditions is satisfied, the rate tuple is achievable.

Since the channel coding rate r_j can be regarded as a scaling coefficient including channel coding rate and the logarithm of the modulation order, we set $r_j = 1$ in this section for simplicity (e.g., with channel coding rate $= \frac{1}{2}$ and quaternary phase shift keying, $r_j = 1$). Other specified parameters are presented in the caption and the legend of each figure.

A. Comparisons Between MAC and Orthogonal Channel

First of all, we make a comparison of the outage probability for different correlation levels between sources through Monte-Carlo methods. The results are shown in Fig. 10. Obviously, the outage probability increases as ρ increases, i.e., the sources are less correlated. As ρ increases from 0.01 to 0.1, the gap between MAC and orthogonal transmission schemes becomes narrower. However, since the gap is already very small, the change of gap is not significant. The reason for the impact of ρ on the gap is that the orthogonal channels provide larger achievable total rate than a MAC, and more correlated sources can better utilize the channel capacity of each channel. Therefore, the transmission of more correlated sources through orthogonal channels has a larger performance

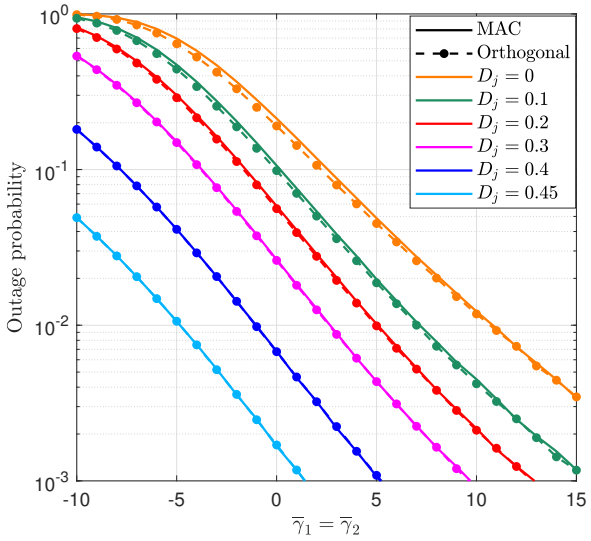

(a) $\rho = 0.01$.

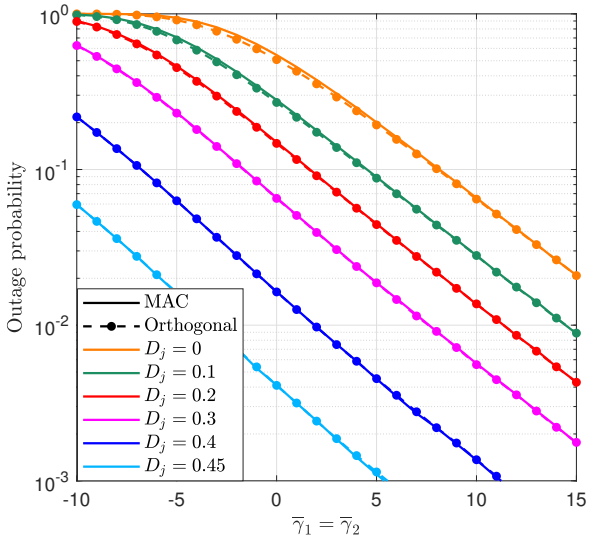

(b) $\rho = 0.1$.

Fig. 10. The impact of $\boldsymbol{\rho}$ on the outage probability for MAC and orthogonal channels, where $\boldsymbol{P_{e2} = 0.1}$ and $\boldsymbol{R_{\text{H}} = 0.5}$.

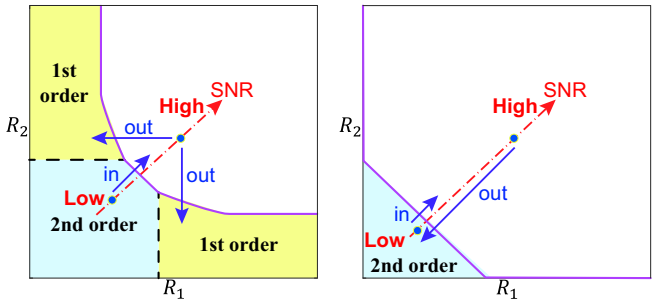

(a) $\rho > 0$. (b) $\rho = 0$.

Fig. 11. The outage region for diverse values of $\boldsymbol{\rho}$.

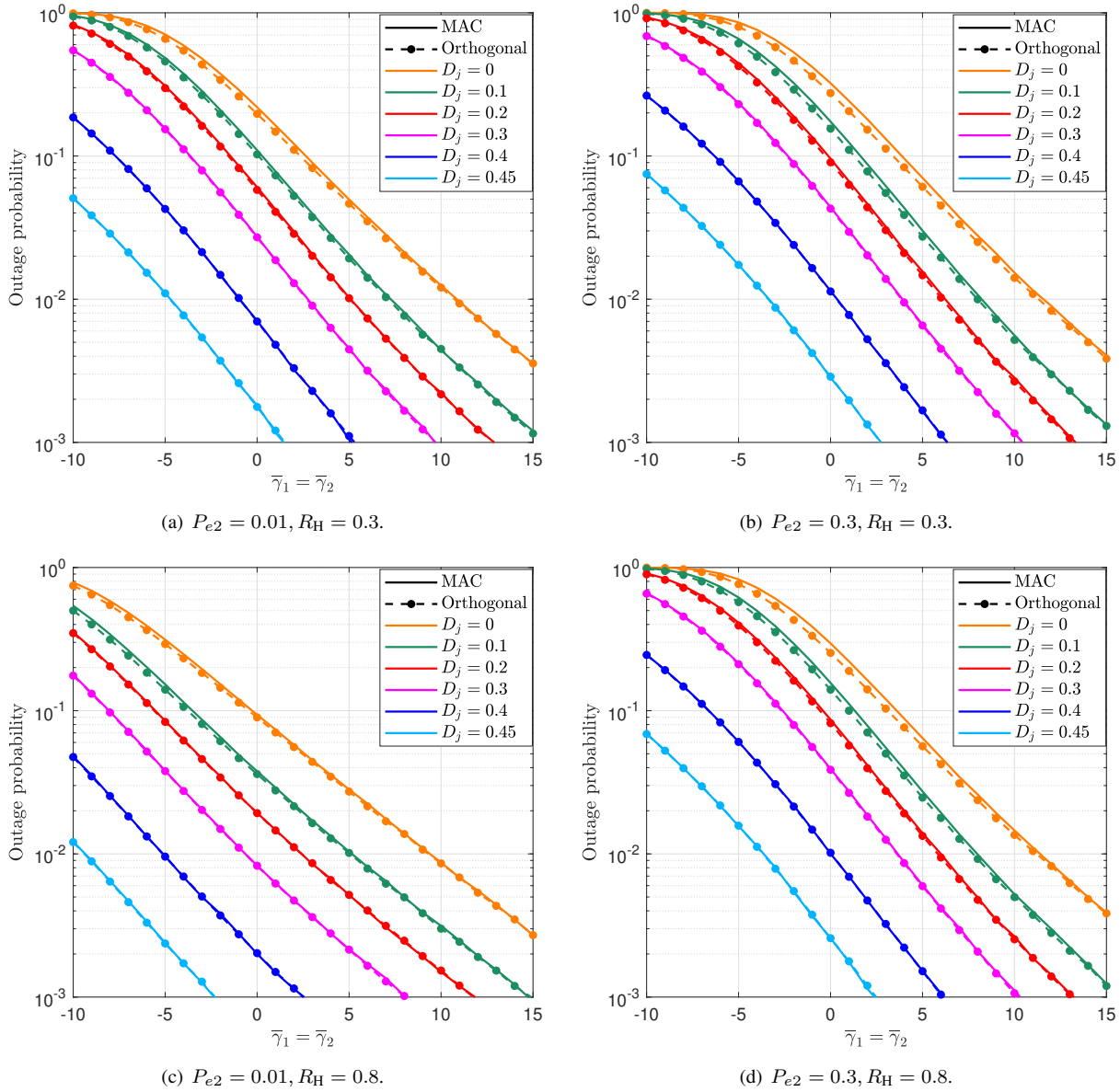

(a) $P_{e2} = 0.01, R_{\mathrm{H}} = 0.3$.

(b) $P_{e2} = 0.3, R_{\mathrm{H}} = 0.3$.

(c) $P_{e2} = 0.01, R_{\mathrm{H}} = 0.8$.

(d) $P_{e2} = 0.3, R_{\mathrm{H}} = 0.8$.

Fig. 12. The impact of $\boldsymbol{P_{e2}}$ and $\boldsymbol{R_{\mathrm{H}}}$ on the outage probability for MAC and orthogonal channels, where $\boldsymbol{\rho = 0.01}$.

gain, i.e., small ρ results in a large gap between MAC and orthogonal channels. Moreover, it is found that the smaller the distortion requirements decrease, the larger the gap occurs between the MAC and the orthogonal schemes. The reason for this observation is because smaller distortion requirements require larger SNR values. However, larger SNR of each link results in larger interference to the other link in MAC, leading to the performance loss, which increases the gap between MAC and orthogonal transmission schemes.

An interesting observation in Fig. 10 is the tendency of the diversity order change. With $\rho = 0.01$, the achieved diversity order is almost two when the required distortion is large, while the diversity order decreases as the required distortion becomes smaller. This is because two sources with $\rho = 0.01$ are almost the same, and the large distortion requirements also provide more error-resistance, resulting in the diversity order close to 2. With smaller distortion requirements, the system is more sensitive to the errors and the differences between two sources, and hence the diversity order decreases. Let assume $\rho = 0.01$ and the distortion requirement is very strict, e.g., $D_i \in [0, 0.1]$, the diversity order reduces and approaches one as the average SNR increases. However, when $\rho = 0.1$, the diversity order is always 1 regardless of the distortion requirements, as shown in Fig. 10(b), even though the crossover probability $\rho = 0.1$ is still small.

In the following, we have a detailed discussion on the reason for the tendency of the diversity order. As illustrated in Fig. 11(a), the outage region for $\rho > 0$ can be divided into three sub-regions. When the average SNR is low, the average rate pair already falls in the outage region. Then, the instantaneous rate pair shifts from the average rate pair, and it may fall into the achievable region if R_1 and/or R_2 increases by a sufficient amount. As the average SNR increases, the instantaneous rate pair can shift into the achievable region

easily due to the contribution of both the links. Therefore, the sub-region of low average SNR corresponds to the second order diversity. Conversely, when the average SNR is high, the average rate pair already falls in the achievable region. However, the reduction of either R_1 or R_2 makes the instantaneous rate pair shift out of the achievable region. Hence, the sub-regions with a low SNR for one link and a high SNR for the other link correspond to the first order diversity. Consequently, the performance gain is dominated by the second and the first order diversities in low and high SNR value ranges, respectively. Nevertheless, in the extreme case of $\rho = 0$, it is easy to show from (11)–(13) that the sub-regions with the first order diversity disappear as shown in Fig. 11(b). Therefore, the diversity order is always two in this case.

Fig. 12 depicts the outage probability for different amount of D_i, P_{e2}, and R_{H} as parameters where P_{e2} and R_{H} values are shown below the figures, indexed by (a)–(d). It is found that the outage probability reduces as P_{e2} decreases and/or R_{H} increases. In addition, the gap between MAC and orthogonal channels becomes larger as P_{e2} increases. The reason for this observation is that when the required SNR increases, the interference and the loss in the achievable rate sum also increase in MAC, resulting in a larger gap between MAC and orthogonal transmission cases. For a very small $P_{e2} = 0.01$, we can find from Fig. 12(a) and Fig. 12(c) that the increase in R_{H} reduces the outage probability. However, if we compare Fig. 12(b) with Fig. 12(d), the performance gain is almost negligible. This is because large P_{e2} indicates that the helper information contains a lot of flipped bits, and hence increasing R_{H} is not effective, even though the source information and the helper information are still correlated. In other words, the helper is not enough correlated to the sources. In this case, the system should allocate more resources to the source-helper link rather than the helper-destination link for a better performance. If R_{H} increases from the value used in Fig. 12(a) to the one in Fig. 12(c), or P_{e2} decreases from the value used in Fig. 12(d) to the one in Fig. 12(c), the diversity order decreases in the low SNR region. This is because the second order sub-region of outages scales down when the helper rate becomes larger or P_{e2} becomes smaller. Then, the first order sub-region dominates the diversity order.

B. Comparisons Between Exact and Approximated Performance for MAC

Now, we compare the outage curves obtained based on the exact rate region by Monte-Carlo methods to that obtained from the approximated rate region by using the numerical integrals. Figs. 13(a), (b) and (c) depict the outage probabilities with $\rho = 0.01$, 0.1 and 0.3, respectively. It is obvious that the approximated result is a lower bound of the outage probability. Moreover, we can observe that as ρ increases, the outage probability increases, while the diversity order and the gap between the exact and approximated results reduce. This is because two sources have lower correlation associated with larger ρ, and hence the achievable region is closer to the case of independent communications, where the shape of the achievable region is not pentagon but rectangular. In particular,

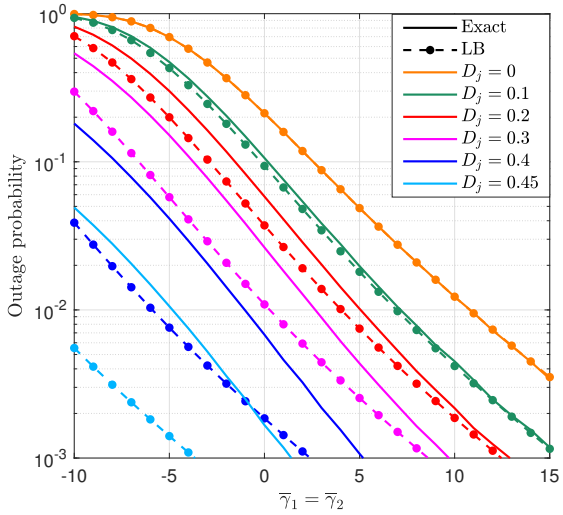

(a) $\rho = 0.01$.

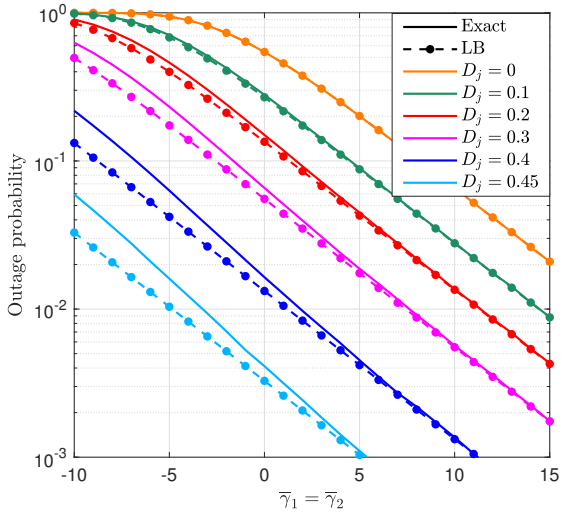

(b) $\rho = 0.1$.

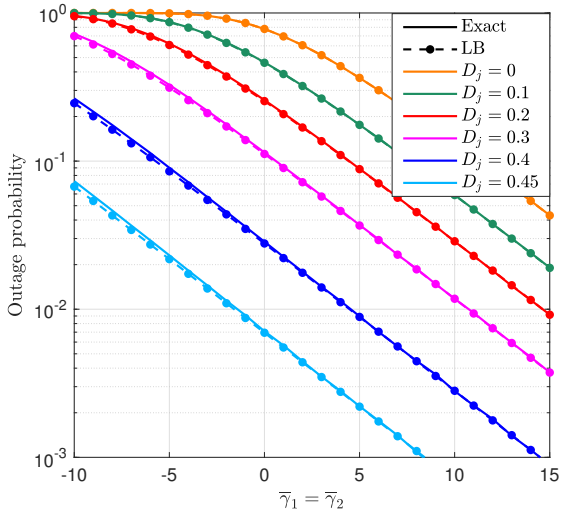

(c) $\rho = 0.3$.

Fig. 13. The impact of $\boldsymbol{\rho}$ on the exact and approximated outage probabilities, where $\boldsymbol{P_{e2} = 0.1}$ and $\boldsymbol{R_{\mathrm{H}} = 0.5}$.

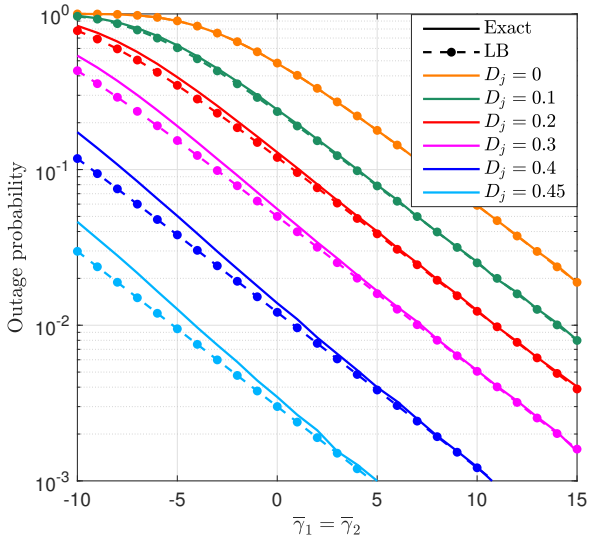

(a) $P_{e2} = 0.01$.

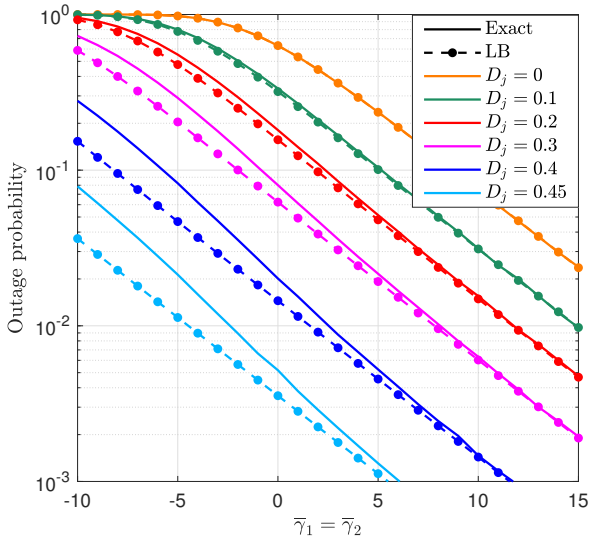

(b) $P_{e2} = 0.3$.

Fig. 14. The impact of $\boldsymbol{P_{e2}}$ on the exact and approximated outage probabilities, where $\boldsymbol{\rho = 0.1}$ and $\boldsymbol{R_{\mathrm{H}} = 0.5}$.

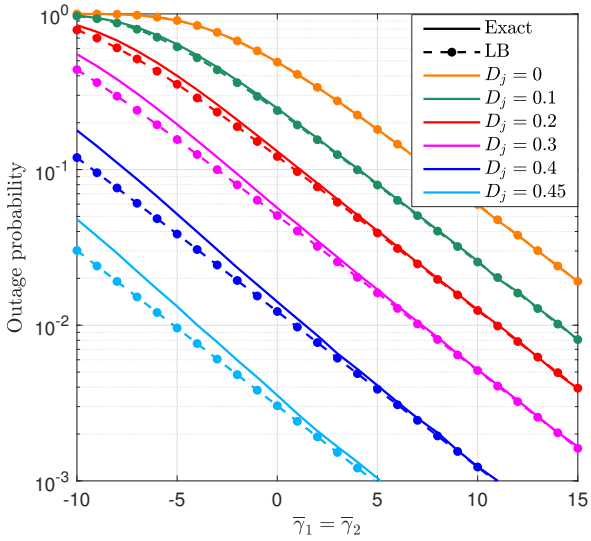

(a) $R_{\mathrm{H}} = 0.8$.

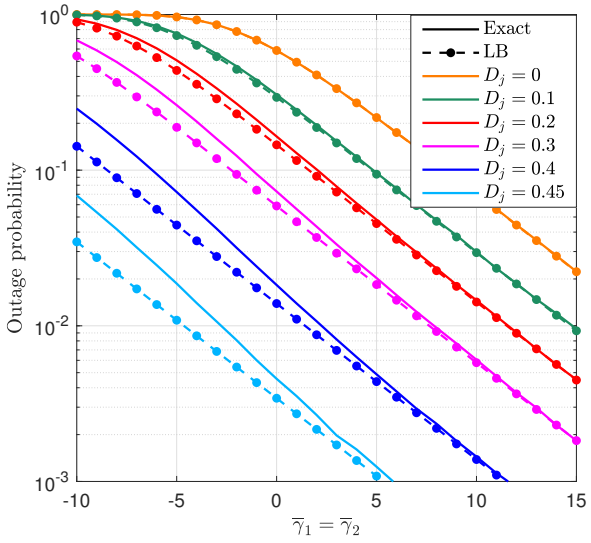

(b) $R_{\mathrm{H}} = 0.3$.

Fig. 15. The impact of $\boldsymbol{R_{\mathrm{H}}}$ on the exact and approximated outage probabilities, where $\boldsymbol{\rho = 0.1}$ and $\boldsymbol{P_{e2} = 0.1}$.

the approximated achievable region becomes rectangular, and is the same as the exact achievable region when $\rho = 0.5$. Therefore, it is obvious that the gap is almost negligible in Fig. 13(c) with $\rho = 0.3$ which is close to 0.5. Nevertheless, the gap between the exact and approximated results also decreases, when the distortion requirement becomes smaller. This is because the approximated achievable region has a closer shape to the exact achievable region with the smaller D_i for $i = 1, 2$. Especially when $D_i = 0$, the communication reduces to lossless, and the approximated achievable region is completely the same as the exact achievable region. Consequently, the two curves coincide with each other when $D_i = 0$. In summary, as ρ changes, significant differences of diversity order and the performance gap can be observed from Fig. 13. It can be concluded that ρ is a dominant parameter on the system performance.

The impact of P_{e2} on the outage probability is illustrated in Fig. 14. It is clearly seen that as P_{e2} becomes larger, the outage event occurs more frequently, and the gap between the exact and the approximated results also becomes wider. The increased gap is caused by the change of the achievable region. The helper information with larger P_{e2} is less effective, and hence the source links require higher rates. Since the minimum required link rates R_1 and R_2 increases, the corner points of the achievable region shift away from each other. Then, the gap between the approximated and exact achievable regions also increases, which affects the gap of the outage probability significantly.

Fig. 15 investigates the impact of R_{H}, and shows the same tendency as Fig. 14. This is obviously because both P_{e2} and R_{H} determine the distortion ρ_V between the helper information and the source information. Provided that ρ_V is kept the same,

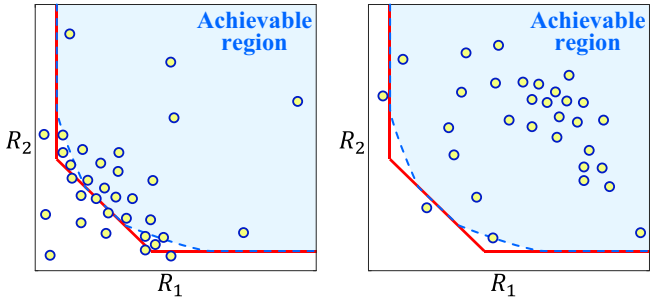

(a) Low average SNR. (b) High average SNR.

Fig. 16. The reason for the gap reduction by increasing the average SNR.

it is easy to find from (24)–(26) that the achievable region does not change. Since $\rho_V = P_{e2} * D_{\mathrm{H}} = P_{e2} * H_b^{-1}(1 - R_{\mathrm{H}})$, the increased P_{e2} has an equivalent effect as decreasing R_{H}.

In addition, it should be noticed that the performance gap decreases as the average SNR becomes larger. We can easily observe this tendency when $D_i \in [0.3, 0.45]$ for $i = 1, 2$. The reason can be explained by Fig. 16. When the average SNR is low, the rate pairs have a high probability to fall into the gap between the approximated and the exact achievable region. Conversely, when the average SNR is large, the rate pairs rarely fall into the gap. The lower probability for falling into the gap of the achievable region results in the narrower performance gap.

C. Comparisons of Lower Bound for Nakagami-m Fading and Optimal Helper

Fig. 17 compares the lower bound between the BF helper and the optimal helper analyzed in [13]. Since the optimal helper can losslessly access two source links, P_{e2} is always 0 with the optimal helper. Hence, we set $P_{e2} = 0$ in Fig. 17 for a better comparison. In the case $P_{e2} > 0$, the outage probability increases only with BF helper. Obviously, there is no doubt that the optimal helper has lower outage probability than the BF helper. It should be noticed that the curve for the optimal helper is not shown for $D_j \geq 0.4$. This is because the optimal helper information is generated by selecting the part of information effective for both source links, i.e., the mutual information between X_1 and X_2. If the source information is recovered by only utilizing the optimal helper information, the distortion can be achieved is $D_j = H_b^{-1}(1 - R_{\mathrm{H}}) \approx 0.316$. Hence, the distortion requirement is already satisfied by the optimal helper for $D_j \geq 0.316$, and the outage probability of the optimal helper reduces to 0 with arbitrary values of $\overline{\gamma}_1$ and $\overline{\gamma}_2$.

Interestingly, in terms of the gap between the BF and the optimal helpers, the gap shown in Fig. 17(a) is larger than Fig. 17(b) for $D_j \leq 0.1$, while Fig. 17(a) shows a smaller gap for $D_j \geq 0.2$. The reason is that the gap is larger if the outage probability is determined more largely by the helper link than the source links. For larger D_j, two source links need to provided less rates compared to the case smaller D_j is required, and the gap is dominated by the helper link. Furthermore, if two sources are less correlated (larger ρ),

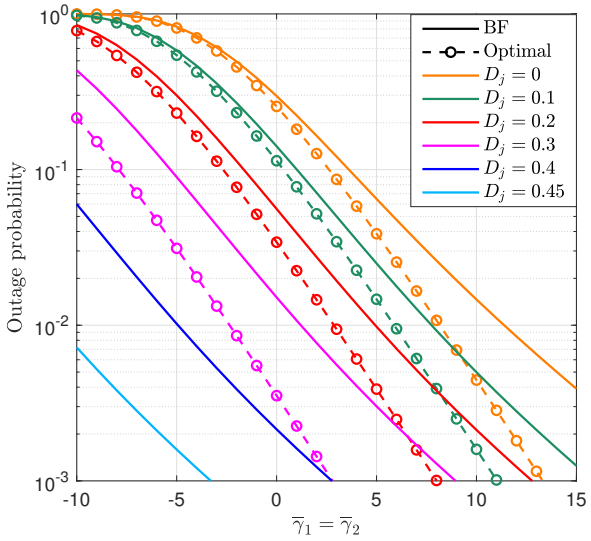

(a) $\rho = 0.01$.

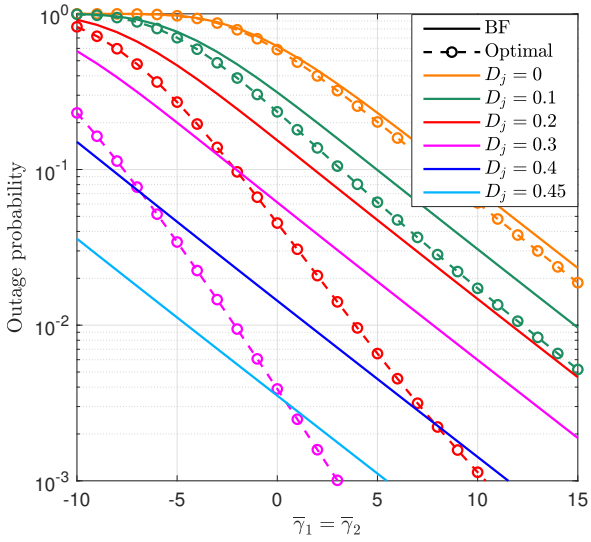

(b) $\rho = 0.1$.

Fig. 17. The comparison of lower bound between BF helper and optimal helper, where $\boldsymbol{P_{e2} = 0}$ and $\boldsymbol{R_{\mathrm{H}} = 0.1}$.

the BF helper will be less effective than the optimal helper, resulting in a larger gap when D_j and ρ are both large. For smaller D_j, the gap is dominated by two source links. In addition, with more correlated sources (smaller ρ), the link rates required for two source links will be reduced, indicating that the helper link determines the gap more in the system. Consequently, the gap is larger when D_j and ρ are both small.

Fig. 18 compares the lower bound with Rayleigh fading to that with Nakagami-m fading. Obviously, the curve with Rayleigh fading perfectly coincides with the curve of Nakagami-m fading with $m = 1$, because Nakagami-m fading reduces to Rayleigh fading when $m = 1$. As m increases, the diversity order under Nakagami-m fading also increases. It can be also found that, with smaller ρ, the diversity order of Nakagami-m fading with $m > 1$ becomes larger than Rayleigh fading.

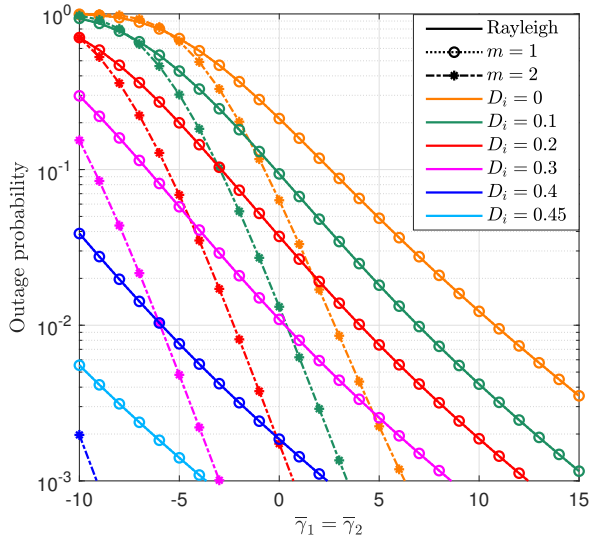

(a) $\rho = 0.01$.

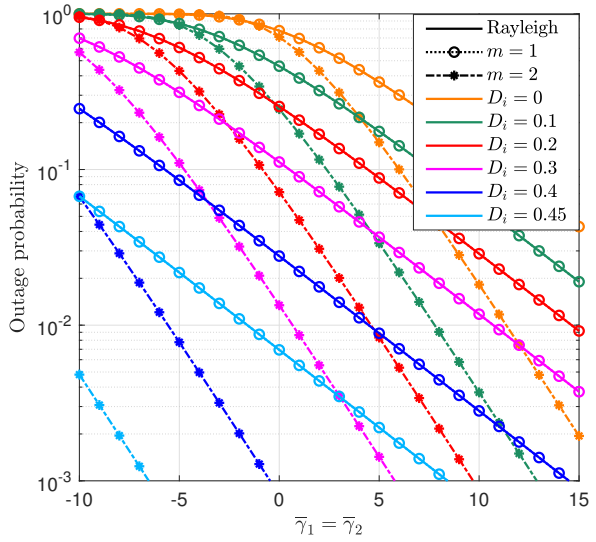

(b) $\rho = 0.3$.

Fig. 18. The comparison of lower bound between Nakagami-$\boldsymbol{m}$ and Rayleigh fading channels, where $\boldsymbol{P_{e2} = 0.1}$ and $\boldsymbol{R_{\mathsf{H}} = 0.5}$.

VI. Conclusion

We have analyzed the rate-distortion and outage probability performances for IoT systems with cooperative lossy communications over MAC assisted by a BF helper. We first characterized the inner bound on the achievable rate-distortion region with two correlated sources and one BF helper. Then, we derived an approximated outage probability theoretically over block Rayleigh or Nakagami-m fading MAC by utilizing the lossy source-channel separation theorem. To verify the accuracy of the theoretical results, and to compare the performance figures between MAC and orthogonal channels, Monte-Carlo methods are utilized to obtain the exact results. It is found that as the required average SNR increases, the transmissions over MAC have larger performance loss than orthogonal channels. Moreover, the diversity order reduces when the average SNR, the crossover probability between sources, and/or the quality of the helper information increase. The approximation based on the theoretical analysis for the outage probability also shows the same tendency as the simulation results. Particularly, the approximated performance results are completely the same as the exact outage probability when the distortion requirement reduces to zero. To present a general view in performance tendency in different scenarios, we have also provided comparisons between Rayleigh and Nakagami-m fading, and between BF helper and optimal helper.

Results of this work could be extended to the following directions. 1) increasing the number of sources and/or helpers; 2) optimizing the sensor placement to achieve a better performance by utilizing the methods presented in [46]–[49]; 3) analyzing the system performance under diverse channel models. They are left as the future work.

Acknowledgment

This paper in part includes intellectual results which the first and the last authors achieved when they were with Japan Advanced Institute of Science and Technology (JAIST) but not published yet, and their extensions. This paper submission has been under the permission by JAIST Research Management Section. The first and the last authors highly appreciate for their official permission, especially for the significant efforts made by Mr. Hiroki Seto.

References

[1] R. Chen, B. Li, and X. Wang, "Multi-camera collaboration for 3D visualization via correlated information maximization," *IEEE Internet of Things Journal*, vol. 11, no. 5, pp. 9127 – 9141, Oct. 2024.

[2] J. Hribar, M. Costa, N. Kaminski, and L. A. DaSilva, "Using correlated information to extend device lifetime," *IEEE Internet of Things Journal*, vol. 6, no. 2, pp. 2439–2448, Apr. 2019.

[3] X. Xu, B. Xu, S. Han, C. Dong, H. Xiong, R. Meng, and P. Zhang, "Task-oriented and semantic-aware heterogeneous networks for artificial intelligence of things: Performance analysis and optimization," *IEEE Internet of Things Journal*, pp. 1–15, Aug. 2023, Early Access.

[4] J. Tang, Y. Zhao, W. Feng, X. Zhao, X. Y. Zhang, M. Liu, and K.-K. Wong, "Cross-layer optimization for industrial internet of things in NOMA-based C-RANs," *IEEE Internet of Things Journal*, vol. 9, no. 18, pp. 16 962–16 975, Sep. 2022.

[5] Y. Xie, B. Lin, Y. Qu, C. Li, W. Zhang, L. Ma, Y. Wen, and D. Tao, "Joint deep multi-view learning for image clustering," *IEEE Transactions on Knowledge and Data Engineering*, vol. 33, no. 11, pp. 3594–3606, Nov. 2021.

[6] J. Li, R. Xu, X. Liu, J. Ma, Z. Chi, J. Ma, and H. Yu, "Learning for vehicle-to-vehicle cooperative perception under lossy communication," *IEEE Transactions on Intelligent Vehicles*, vol. 8, no. 4, pp. 2650–2660, Apr. 2023.

[7] M. Raginsky, "Learning from compressed observations," in *IEEE Information Theory Workshop*, Tahoe City, CA, USA, Sep. 2007, pp. 420–425.

[8] G. Katz, P. Piantanida, R. Couillet, and M. Debbah, "On the necessity of binning for the distributed hypothesis testing problem," in *IEEE International Symposium on Information Theory (ISIT)*, Hong Kong, China, Jun. 2015, pp. 2797–2801.

[9] P. A. Stavrou and M. Kountouris, "A rate distortion approach to goal-oriented communication," in *IEEE International Symposium on Information Theory (ISIT)*, Espoo, Finland, Jun. 2022, pp. 590–595.

[10] W. Lin, S. Qian, and T. Matsumoto, "Lossy-forward relaying for lossy communications: Rate-distortion and outage probability analyses," *IEEE Transactions on Wireless Communications*, vol. 18, no. 8, pp. 3974–3986, Aug. 2019.

[11] W. Lin and T. Matsumoto, "An analysis of performance improvement by a helper for wireless sensor networks," in *IEEE 29th Annual International Symposium on Personal, Indoor and Mobile Radio Communications (PIMRC)*, Bologna, Italy, Sep. 2018.

[12] ——, "Performance analysis of distortion-acceptable cooperative communications in wireless sensor networks for Internet of Things," *IEEE Sensors Journal*, vol. 19, no. 5, pp. 1979–1989, Mar. 2019.

[13] W. Lin, Q. Xue, J. He, M. Juntti, and T. Matsumoto, "Rate-distortion and outage probability analyses for single helper assisted lossy communications," *IEEE Transactions on Vehicular Technology*, vol. 68, no. 11, pp. 10 882–10 894, Nov. 2019.

[14] Y. Oohama, "Rate-distortion theory for Gaussian multiterminal source coding systems with several side informations at the decoder," *IEEE Transactions on Information Theory*, vol. 51, no. 7, pp. 2577–2593, 2005.

[15] A. Wyner and J. Ziv, "The rate-distortion function for source coding with side information at the decoder," *IEEE Transactions on information Theory*, vol. 22, no. 1, pp. 1–10, Jan. 1976.

[16] R. Timo, T. Chan, and A. Grant, "Rate distortion with side-information at many decoders," *IEEE Transactions on Information Theory*, vol. 57, no. 8, pp. 5240–5257, Aug. 2011.

[17] A. Sechelea, A. Munteanu, S. Cheng, and N. Deligiannis, "On the rate-distortion function for binary source coding with side information," *IEEE Transactions on Communications*, vol. 64, no. 12, pp. 5203–5216, Dec. 2016.

[18] T. Berger, "Multiterminal source coding," in *The Information Theory Approach to Communications, G. Longo, Ed.* New York: Springer-Verlag, 1978, pp. 171–231.

[19] S. Y. Tung, "Multiterminal source coding," Ph.D. dissertation, School of Electrical Engineering, Cornell University, Ithaca, New York, 1978.

[20] F. Shirani and S. S. Pradhan, "A new achievable rate-distortion region for distributed source coding," *IEEE Transactions on Information Theory*, vol. 67, no. 7, pp. 4485–4503, Jul. 2021.

[21] L. Xie, X. Tu, S. Zhou, and J. Chen, "Generalized gaussian multiterminal source coding in the high-resolution regime," *IEEE Transactions on Communications*, vol. 68, no. 6, pp. 3782–3791, Jun. 2020.

[22] Y. Yang and Z. Xiong, "On the generalized Gaussian CEO problem," *IEEE Transactions on Information Theory*, vol. 58, no. 6, pp. 3350–3372, Jun. 2012.

[23] Y. Oohama, "Gaussian multiterminal source coding," *IEEE Transactions on Information Theory*, vol. 43, no. 6, pp. 1912–1923, Nov. 1997.

[24] ——, "The rate-distortion function for the quadratic Gaussian CEO problem," *IEEE Transactions on Information Theory*, vol. 44, no. 3, pp. 1057–1070, May 1998.

[25] ——, "Indirect and direct Gaussian distributed source coding problems," *IEEE Transactions on Information Theory*, vol. 60, no. 12, pp. 7506–7539, Dec. 2014.

[26] B. Schein and R. Gallager, "The Gaussian parallel relay network," in *IEEE International Symposium on Information Theory*, Sorrento, Italy, Jun. 2000, pp. 22–22.

[27] T. M. Cover and J. A. Thomas, *Elements of information theory*, 2nd ed. John Wiley & Sons, 2012.

[28] J. He, V. Tervo, X. Zhou, X. He, S. Qian, M. Cheng, M. Juntti, and T. Matsumoto, "A tutorial on lossy forwarding cooperative relaying," *IEEE Communications Surveys & Tutorials*, vol. 21, no. 1, pp. 66–87, First quarter 2018.

[29] C. E. Shannon, "A mathematical theory of communication," *Bell System Technical Journal*, vol. 27, no. 3, pp. 379–423, Jul. 1948.

[30] ——, "Coding theorems for a discrete source with a fidelity criterion," *IRE Nat. Conv. Rec*, vol. 4, no. 1, pp. 142–163, Mar. 1959.

[31] J. Garcia-Frias and Y. Zhao, "Near-Shannon/Slepian-Wolf performance for unknown correlated sources over AWGN channels," *IEEE Transactions on Communications*, vol. 53, no. 4, pp. 555–559, Apr. 2005.

[32] J.-J. Xiao and Z.-Q. Luo, "Multiterminal source–channel communication over an orthogonal multiple-access channel," *IEEE Transactions on Information Theory*, vol. 53, no. 9, pp. 3255–3264, Sep. 2007.

[33] J. Harshan and E. Viterbo, "Constellation constrained capacity of additive Gaussian mixture noise channels," in *International Symposium on Information Theory and its Applications*, Victoria, BC, Canada, Oct. 2014, pp. 110–114.

[34] A. El Gamal and Y.-H. Kim, *Network information theory*. Cambridge University Press, 2011.

[35] A. Padakandla, "Communicating correlated sources over MAC and interference channels I: Separation-based schemes," *IEEE Transactions on Information Theory*, vol. 66, no. 7, pp. 4104–4128, 2020.

[36] S. Song, J. He, and T. Matsumoto, "Rate-distortion and outage probability analyses of Wyner-Ziv systems over multiple access channels," *IEEE Transactions on Communications*, vol. 69, no. 9, pp. 5807–5816, Sep. 2021.

[37] G. Im and J. H. Lee, "Outage probability for cooperative NOMA systems with imperfect SIC in cognitive radio networks," *IEEE Communications Letters*, vol. 23, no. 4, pp. 692–695, Apr. 2019.

[38] X. Liang, Y. Wu, D. W. K. Ng, S. Jin, Y. Yao, and T. Hong, "Outage probability of cooperative NOMA networks under imperfect CSI with user selection," *IEEE Access*, vol. 8, pp. 117 921–117 931, May 2020.

[39] W. Lin, L. Li, J. Yuan, Z. Han, M. Juntti, and T. Matsumoto, "Cooperative lossy communications in unmanned aerial vehicle networks: Age-of-information with outage probability," *IEEE Transactions on Vehicular Technology*, vol. 70, no. 10, pp. 10 105–10 120, Oct. 2021.

[40] J. Chen, D. Qiao, and H. Qian, "Outage analysis of relay-assisted mmWave cellular systems employing JSDM," *IEEE Access*, vol. 7, pp. 60 793–60 805, May 2019.

[41] S. Qian, J. He, X. Zhou, T. Imai, and T. Matsumoto, "Outage analysis for correlated sources coding over NOMA in shadowed κ-μ fading," in *IEEE Wireless Communications and Networking Conference (WCNC)*, Austin, TX, USA, Apr. 2022, pp. 1999–2004.

[42] A. Papoulis and S. U. Pillai, *Probability, random variables, and stochastic processes*, 4th ed. New York: McGraw-Hill, 2002.

[43] X. Zhou, M. Cheng, X. He, and T. Matsumoto, "Exact and approximated outage probability analyses for decode-and-forward relaying system allowing intra-link errors," *IEEE Transactions on Wireless Communications*, vol. 13, no. 12, pp. 7062–7071, Dec. 2014.

[44] I. S. Gradshteyn and I. M. Ryzhik, *Table of integrals, series, and products*, 7th ed., A. Jeffrey and D. Zwillinger, Eds. Burlington, MA: Academic Press, 2007.

[45] A. Barbu and S.-C. Zhu, *Monte Carlo Methods*. Singapore: Springer, 2020.

[46] Q. Shi, X. Wang, W. Chen, and K. Hu, "Optimal sensor placement method considering the importance of structural performance degradation for the allowable loadings for damage identification," *Applied Mathematical Modelling*, vol. 86, pp. 384–403, Oct. 2020.

[47] C. Yang and Y. Xia, "Interval Pareto front-based multi-objective robust optimization for sensor placement in structural modal identification," *Reliability Engineering & System Safety*, vol. 242, p. 109703, Feb. 2024.

[48] Q. Shi, H. Wang, L. Wang, Z. Luo, X. Wang, and W. Han, "A bilayer optimization strategy of optimal sensor placement for parameter identification under uncertainty," *Structural and Multidisciplinary Optimization*, vol. 65, no. 9, p. 264, Sep. 2022.

[49] C. Yang, "Interval strategy-based regularization approach for force reconstruction with multi-source uncertainties," *Computer Methods in Applied Mechanics and Engineering*, vol. 419, p. 116679, Feb. 2024.